Excited State Dynamics of Ag Atoms in Helium Nanodroplets†

Evgeniy Loginov and Marcel Drabbels*

Laboratoire de Chimie Physique Moléculaire, Ecole Polytechnique Fédéral de Lausanne (EPFL), CH-1015 Lausanne, Switzerland

Received: February 27, 2007; In Final Form: April 27, 2007

The excited state dynamics of silver atoms embedded in helium nanodroplets have been investigated by a variety of spectroscopic techniques. The experiments reveal that 5p $^2P_{1/2} \leftarrow$ 5s $^2S_{1/2}$ excitation of embedded silver atoms results almost exclusively in the ejection of silver atoms populating the $^2P_{1/2}$ state. In contrast, excitation to the 5p $^2P_{3/2}$ state leads to the ejection of not only silver atoms in the $^2P_{1/2}$, $^2P_{3/2}$, and $^2D_{5/2}$ excited states but also of AgHe and $AgHe_2$. These AgHe exciplexes are mainly formed in the $A^2\Pi_{1/2}$ electronic state. In addition, it is found that a considerable fraction of the $^2P_{3/2}$ excited silver atoms become solvated within the helium droplets, most probably as $AgHe_2$. The observations can be accounted for by a model in which the metastable $^2D_{5/2}$ state of silver acts as a doorway state in the relaxation of $^2P_{3/2}$ excited silver atoms.

1. Introduction

The systematic spectroscopic interrogation of foreign species immersed into helium nanodroplets has proven to be a powerful way to probe the microscopic properties of this quantum liquid. As a result, helium droplets have attracted considerable interest from both experimentalists and theoreticians alike.[1−7] The use of helium nanodroplets for the investigation of chemical reactions is currently being actively discussed in the literature. The droplets' ability to stabilize weakly bound species can be exploited to probe for example entrance and exit channel complexes, or possibly even reaction intermediates. Although some first experiments have been performed,[8−12] the field is still largely unexplored and many questions remain to be answered. One of the central questions relates to the cooling of reaction intermediates and products by the helium environment. Recent experiments have provided first estimates for the cooling rates of the vibrational degrees of freedom in helium droplets. Although a cooling mechanism has been proposed, a detailed and consistent picture is still lacking.[13−16] Even less is known on the cooling of the translational degree of freedom. Recently we have started to systematically study the translational dynamics of species in helium droplets.[17,18] The first experiments in our laboratory employed photodissociation of alkyl iodides to create species inside helium nanodroplets with a well-defined kinetic energy. By comparing the velocity distribution of photofragments that have escaped from the droplets with the initial speed distribution of the fragments, the mechanism responsible for the kinetic energy transfer could be inferred. It was concluded that the translationally highly energetic fragments lose their kinetic energy mainly by binary collisions with individual helium atoms making up the liquid. These results appear to be consistent with observations made by other groups and with recent calculations.[14,19,20] As the speeds of most fragments in these experiments exceed by far the so-called critical Landau velocity, the velocity below which no elementary excitations of the helium can be generated,[21] these experiments did not probe the translational dynamics in the velocity regime where superfluidity is thought to have the largest impact.

The molecular species used in our previous experiments[17,18] are thought to have weak but attractive interactions with the helium environment and consequently will be solvated in the helium droplets. However, in chemical reactions often radicals and species in electronically excited states are produced that have a repulsive interaction with the helium. As a result, it is energetically not favorable for these species to be solvated in the droplets. Accordingly, they will be transported toward the surface where they might bind due to the long range attractive forces[22] or be ejected from the droplet. To address the issues related to the motion of these types of species, we have started a systematic investigation of the dynamics of optically excited silver atoms in helium droplets.

The first spectroscopic identification of silver atoms in liquid helium was reported in 1995 by the group of Takami.[23] In these experiments, silver atoms were introduced into bulk liquid helium by laser ablation and subsequently probed by laser-induced fluorescence. The excitation spectra revealed that the D1 transition, corresponding to 5p $^2P_{1/2} \leftarrow$ 5s $^2S_{1/2}$ excitation, of the dissolved silver atoms was substantially broadened and shifted by several nanometers to the blue with respect to the gas phase. This observation could be explained within the framework of the spherical atomic bubble model introduced earlier to explain the excitation and fluorescence spectra of alkaline earth atoms in liquid and solid helium.[24−26] In contrast, the D2 transition, corresponding to excitation to the 5p $^2P_{3/2}$ state, was not observed in this study. Later experiments employing dispersed fluorescence spectroscopy revealed that excitation via the D2 transition gives rise to emission via the D1 transition, indicating that fast nonradiative relaxation from the $^2P_{3/2}$ to $^2P_{1/2}$ state must occur.[27] In addition, the dispersed fluorescence spectra revealed a broad emission that is substantially shifted to the red of the excitation wavelength. With the help of high level ab initio calculations, this fluorescence was proven to originate from the excited $\tilde{A}^2\Pi_{3/2}$ state of $AgHe_2$ that correlates to the $^2P_{3/2}$ state of the silver atom. Later experiments by Takami and co-workers on the radiative lifetime of silver atoms in dense helium gas at temperatures around the critical temperature provided convincing evidence that under those

† Part of the "Roger E. Miller Memorial Issue".

* Corresponding author. E-mail: Marcel.Drabbels@epfl.ch.

10.1021/jp0716278 CCC: $37.00
Published on Web 06/15/2007

conditions the relaxation of $^2P_{3/2}$ excited silver atoms occurs via the $^2D_{5/2}$ state.[28]

For the bulk experiment, it is evident that the silver atoms are dissolved by the helium. However, in the case of helium droplets the location of the silver atoms is not known a priori. The electronic structure of silver is similar to that of alkali metal atoms. One might therefore expect that the silver atoms, analogous to the alkali metals, are located at the surface.[22] However, the beam depletion spectra of silver-doped helium droplets obtained by Toennies and co-workers closely resembled the electronic excitation spectrum of silver atoms in bulk helium.[29] This was taken as evidence that silver atoms, in contrast to alkali metal atoms, reside in the interior of the droplets. Shortly thereafter, experiments on silver doped helium droplets that used a laser ionization based detection scheme revealed that, following electronic excitation via the D2 transition, silver atoms are being ejected from the droplets.[30] It was furthermore observed that these ejected silver atoms mainly populated the $^2P_{1/2}$ electronic state. Quantum Monte Carlo calculations on $AgHe_N$ clusters following this experimental work confirmed the solvation of ground state silver atoms in helium droplets.[31] Furthermore, the calculations could largely reproduce the experimentally observed excitation spectra. On the basis of this successful simulation of the spectra, it was proposed that the $^2P_{1/2} \leftarrow {}^2P_{3/2}$ relaxation observed both in bulk helium and in helium droplets is due to a vibronic coupling of the excited states involved. In contrast to these calculations, more recent quantum molecular dynamics simulations indicate that helium induced nonadiabatic transitions between three electronic states during the first few hundred femtoseconds after excitation are responsible for the observation of Ag $^2P_{1/2}$ after excitation via the D2 transition.[32] The simulations furthermore convincingly showed that, following optical excitation, helium atoms are expelled from the region around the silver atom and that a bubble structure forms on a picosecond time scale. In some cases, $AgHe_N$ exciplexes with $N \leq 5$ formed inside the bubble, indicating a possible solvation of these structures.

In the current set of experiments, we have investigated the excited state dynamics of Ag doped helium droplets by employing a variety of experimental techniques, ranging from zero electron kinetic energy (ZEKE) spectroscopy to ion imaging. These measurements allow us to verify some of the models put forward to explain the efficient $^2P_{3/2} \rightarrow {}^2P_{1/2}$ relaxation of silver atoms in liquid helium and to gain more insight into the excited state dynamics of silver atoms in liquid helium droplets. As such, these experiments serve as a starting point for the investigation of the translation dynamics of photoexcited silver atoms in helium nanodroplets, on which we will report in a forthcoming publication.

2. Experiment

The experimental setup has recently been described in great detail.[18] Only the most relevant features will be given here. Helium droplets are formed by expanding high-purity ^{4}He gas (99.9999%) at a pressure of typically 30 bar into vacuum through a 5 μm orifice cooled by a closed-cycle refrigerator to temperatures in the range of 9−20 K. This temperature range gives access to both the subcritical and the supercritical expansion regime and thereby allows for the production of a wide range of droplet sizes.[2,33,34] Via a conical skimmer the droplet beam enters a second vacuum stage that accommodates a high-temperature oven. High-purity silver (99.999%, Goodfellow) placed in the oven is heated up to 800 °C to create a silver vapor over a length of 30 mm. The oven temperature is adjusted for every droplet size to ensure that the droplets on average pick up less than one silver atom as they pass through the vapor. After an additional differential pumping stage, the beam of doped droplets enters the main vacuum chamber, which holds an ion imaging setup. The embedded silver atoms are excited to the 5p state by crossing the droplet beam at the center of an imaging setup with the frequency-doubled output of a Nd:YAG pumped dye laser (PrecisionScan, Sirah Laser- und Plasmatechnik GmbH). The silver atoms are subsequently further excited or ionized by the absorption of an additional photon. In most of the experiments described here this second photon is provided by the counterpropagating frequency-doubled output of another Nd:YAG pumped dye laser (TDL 50, Quantel International). Both dye lasers are fired simultaneously at a repetition rate of 20 Hz, and the polarization of the two laser beams is adjusted to be parallel to the molecular beam axis. To cover the relevant wavelength region between 300 and 340 nm, the dye lasers are operated with Pyrromethene 597 or DCM and their output is frequency doubled in a KDP crystal. The ions or electrons created are projected using an electrostatic asymmetric immersion lens onto a position-sensitive detector that consists of two 75 mm diameter microchannel plates (MCP) and a phosphor screen. The flight path from the lens to the detector of about 40 cm is shielded from the stray magnetic fields by a high-permeability foil. The electrical signal from the phosphor screen is fed into an oscilloscope and a multichannel scaler (P7886, FAST ComTec GmbH) which offers the possibility to record ion time-of-flight mass spectra. The light emitted by the phosphor screen is imaged onto a CCD camera interfaced to a PC. In our previous studies a cooled CCD camera was used which was read out after a typical exposure time of 1 h. For the experiments described here, this camera has been replaced by a high-resolution (1k × 1k) machine vision CCD camera (A200, Basler AG) which is read out every laser shot. The individual images are analyzed online, and the centroids of the ion or electron impacts are determined with single pixel resolution. High-resolution ion or electron images are constructed by adding together the centroids of individual images collected during typically 1 h. By gating the voltage applied to the front of the detector, ion images can be recorded for a specific mass. The three-dimensional velocity distribution of the ions, or alternatively electrons, is finally derived from the recorded two-dimensional images by applying an inverse Abel transform to the images.[35,36] With the previously used cooled CCD camera, excitation spectra could only be obtained by reading out the electrical signal from the phosphor screen. With the new camera setup, it is now possible to record spectra by counting the number of ions or electrons hitting the detector at a specific wavelength. As a result, excitation spectra can be recorded with much higher signal-to-noise ratio than before.

In the present study, various spectroscopic and imaging techniques have been utilized to investigate the dynamics of photoexcited silver atoms. All these techniques use the same imaging setup, which consists of a repeller plate, an open extractor, and an open ground electrode. Since each type of measurement requires a different set of voltages to be applied to the electrodes, we will give here a short description of the settings used.

To determine the products formed by exciting the embedded silver atoms, time-of-flight mass spectra have been recorded. This has been achieved by applying static positive voltages to the repeller and extractor electrodes (the ratio for time focusing being 1:0.85) and integrating the arrival times of ions at the detector during typically 30 min using the multichannel scaler.

At the typical repeller voltage of 500 V used in the present experiments, the time resolution is limited by the capacitance of the detector to 20 ns, which is sufficient to resolve the ^{107}Ag and ^{109}Ag isotopes. The maximum mass that can be detected with the present setup is limited by the fact that the imaging setup is mounted perpendicular to the droplet beam axis. For helium droplet beams formed under our experimental conditions, it has been possible to detect masses up to approximately 50 000 amu by applying 8 kV to the repeller and the corresponding voltage to the extractor.

To determine the velocity distributions of the products, velocity map images have been recorded by applying slightly different static positive voltages to the repeller and extractor electrodes (voltage ratio 1:0.707). The images are typically recorded by applying 500 V to the repeller and the corresponding voltage to the extractor and using an integration time of 1 h. By performing an inverse Abel transformation on the resulting high-quality images, the speed distributions of the products could be determined with a resolution of 4 m/s. The use of conventional ion imaging in the present study has one serious drawback. Since the species are ionized in a non-state-specific way, it is impossible to determine the velocity distributions of products in different quantum states. However, by using conditions usually encountered in mass analyzed threshold ionization (MATI) spectroscopy,[37] it becomes feasible to record quantum-state-specific ion images. In the presence of a small electric field produced by applying 500 and 400 V to repeller and extractor respectively, the frequency of the second laser is set to excite products in one specific quantum state to Rydberg states close to the ionization threshold. Typically 2 μs after firing of the lasers, the voltages applied to the repeller and extractor are increased to the values appropriate for velocity map imaging. The Rydberg atoms are field ionized by the increased electric field and the resulting ions are imaged onto the detector, which is gated at the arrival time of the mass of interest. The delay time between the firing of the lasers and the switching of the voltages is sufficiently long that any ions formed by direct ionization have left the volume that is being imaged. The spectral resolution that can be achieved by this version of ion imaging is largely determined by the applied voltages. With the setting typically used in these experiments, a spectral resolution of 10 cm^{-1} is readily attained.

Whereas time-of-flight mass spectrometry has been used to determine the products that are formed, photoelectron spectroscopy has been applied to determine the state distributions of these products. Electron images are recorded by applying static negative voltages to the repeller and extractor electrodes with a voltage ratio identical to that for ion imaging (1:0.707). By applying an inverse Abel transform to the recorded electron images, the corresponding photoelectron spectra can be obtained. At the typical repeller voltage of -500 V, an energy resolution of 3% is achieved for the photoelectrons. Because the resolution is limited and, as we will show below, not sufficient to resolve all transitions in these experiments, we have also used the setup to perform ZEKE spectroscopy.[38] In these experiments, the silver products formed by the first laser are excited to high Rydberg states by the second laser while a voltage of $+0.1$ V is applied to the repeller and the extractor is being kept at ground. Electrons formed by direct ionization of the silver products are removed from the detection volume by this small electric field. Typically, 2 μs after firing of the lasers the voltage on the repeller is adjusted to -1.0 V. This field ionizes the high Rydberg states and accelerates the electrons to the detector, where they are counted. In this way, ZEKE spectra have been recorded with 2 cm^{-1} resolution.

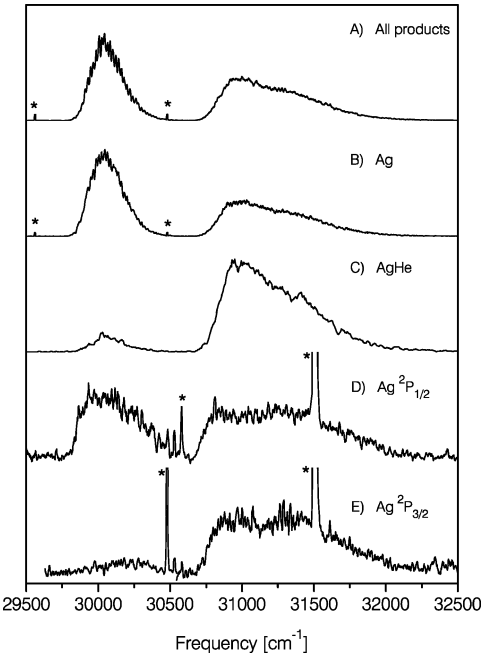

Figure 1. Excitation spectrum of silver atoms embedded in helium nanodroplets with a mean radius of 41 Å recorded by monitoring all products (A), only silver atoms (B), AgHe exciplexes (C), Ag atoms in the 5p $^2P_{1/2}$ state (D), and Ag atoms in the 5p $^2P_{3/2}$ state (E). The lines indicated with asterisks originate from gas-phase silver atoms present in the detection region.

3. Results

3.1. Excitation Spectra. We start our presentation of the results by discussing the excitation spectra. Figure 1 shows various excitation spectra of silver atoms embedded in helium droplets with a mean radius of 41 Å. The upper spectrum is recorded by scanning the excitation laser over the wavelength region 305−340 nm while the wavelength of the second laser was kept fixed at 292.5 nm. The energy of the second photon is sufficient to ionize not only silver atoms irrespective of their quantum state ($^2P_{1/2}$, $^2D_{5/2}$, or $^2P_{3/2}$) but also any $AgHe_N$ clusters that are possibly formed. At the same time, this wavelength is not being absorbed by the embedded silver atoms. To avoid saturation of the transitions and to minimize the background resulting from one-color excitation and ionization, the fluence of the excitation laser was kept below 0.5 mJ/cm^2. The created ions are accelerated by the applied electric field toward the detector, and the total number of ions is determined at each wavelength. It should be mentioned that the resulting excitation spectrum does not necessarily represent the absorption spectrum of the embedded silver atoms. Since the detection efficiency of the microchannel plates is mass-dependent and consequently silver ions embedded in helium droplets are much less efficiently detected than free silver ions, the excitation spectrum shown is strongly biased for excitation to those levels that produce free silver atoms or small $AgHe_N$ clusters. Inspection of the spectrum shown in Figure 1 reveals that it consists of two bands that can readily be assigned to the D1 and D2 transitions of the dissolved silver atoms. The shape of these bands is largely independent of droplet size and agrees fairly well with the beam depletion spectrum as measured by Bartelt et al.[29] Whereas it is difficult to judge from the beam depletion spectra whether the intensity between the bands goes to zero or the bands partially overlap,

the present spectrum clearly shows that the two bands are fully separated. The relative intensities of the two bands are found to show a slight dependence on droplet size; i.e., the relative intensity of the band corresponding to excitation to the $^2P_{3/2}$ level increases with decreasing droplet size. Since the spectrum is composed of contributions of various species, this droplet size dependence might well reflect the variation of these contributions with droplet size. We therefore have recorded the excitation spectra corresponding to ^{107}Ag and ^{109}AgHe by gating the detector at the arrival times of the corresponding masses. By choosing these two masses, contamination of the signal by contributions of neighboring masses could be minimized. The resulting spectra are also displayed in Figure 1. Whereas the spectrum recorded by detecting Ag atoms corresponds very closely to that obtained by collecting all ions, the spectrum resulting from the detection of AgHe is markedly different. Although the shape of the two bands is identical to that in the Ag excitation spectrum, the relative intensities are clearly very different. Apparently, AgHe is mainly formed by excitation to the $^2P_{3/2}$ state. It was furthermore found that that the absolute signal level of the AgHe excitation spectrum was strongly droplet size dependent, with smaller droplets yielding more AgHe. These findings together explain the observed weak droplet size dependence of the relative intensities of both bands in the excitation spectrum recorded by integrating the signal of all masses. Attempts to record excitation spectra for other $AgHe_N$ products were not successful, even though some of these products are observed in the time-of-flight mass spectra; see below.

The Ag excitation spectrum clearly reveals two bands that have almost equal intensity and correspond to excitation to the $^2P_{1/2}$ and $^2P_{3/2}$ states of the dissolved silver atoms, in agreement with calculations.[31,32] According to the quantum Monte Carlo simulations the final state distribution of the silver atoms should depend only weakly on the transitions used in the excitation.[32] To verify this, we have recorded excitation spectra corresponding to free silver atoms in the $^2P_{1/2}$ and $^2P_{3/2}$ quantum states. This has been achieved by scanning the wavelength of the first laser and applying a detection scheme usually encountered in MATI spectroscopy and described in more detail in the experimental section. Since the wavelengths used in the second step are within the absorption profile of the embedded silver atoms, the intensity of the second laser had to be kept sufficiently low to prevent contributions to the signal arising from excitation by the second laser. Consequently, this detection scheme is significantly less sensitive than that used to record the non-state-specific excitation spectra. To make up for this loss in sensitivity and to be able to record spectra with a sufficient signal-to-noise ratio, the fluence of the excitation laser was increased to 10 mJ/cm^2. The resulting state-specific excitation spectra are also depicted in Figure 1. The Ag $^2P_{1/2}$ excitation spectrum is quite similar to the overall silver spectrum. The D1 and D2 transitions appear with almost equal intensity but are somewhat broader than in the non-state-specific spectra. This broadening can be attributed to the saturation of the excitation transition by the high laser fluence used. The Ag $^2P_{3/2}$ excitation spectrum shows the same two bands. However, analogous to the AgHe spectrum, the D2 transition is more intense. Based on these observations, it becomes clear that excitation via the D1 transition leads mainly to the ejection of Ag atoms in the $^2P_{1/2}$ state. In contrast, excitation via the D2 transition produces silver atoms in both the $^2P_{1/2}$ and $^2P_{3/2}$ states as well as AgHe. In spite of the high laser fluence, it was not possible to record a state-specific $^2D_{5/2}$ excitation spectrum with sufficient signal-to-noise ratio, although, as we will show below, silver atoms are produced in this state.

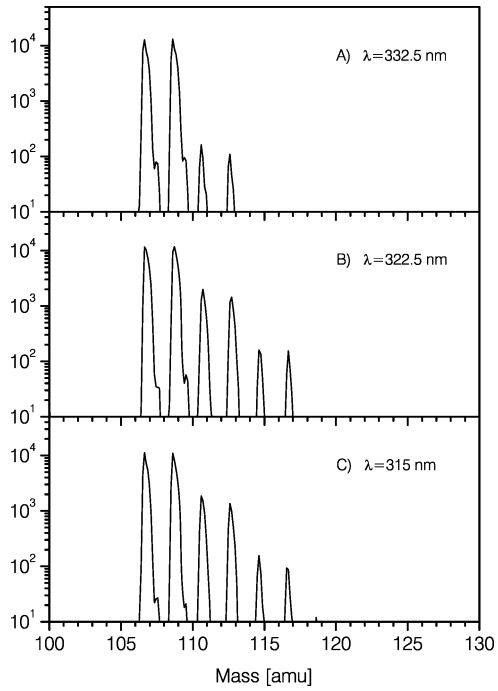

Figure 2. Time-of-flight mass spectra recorded following excitation of silver atoms via the D1 transition at a wavelength of 332.5 nm (A) and via the D2 transition at 322.5 (B) and 315 nm (C). The silver atoms are embedded in helium droplets with a mean radius of 41 Å.

3.2. Time-of-Flight Mass Spectra. The experiments described above show that the excitation of silver atoms embedded in helium droplets yields not only free silver atoms but also AgHe exciplexes. The experiments furthermore indicated that the number of AgHe products formed is related to the helium droplet size. To investigate this in a more systematic way, we have recorded a series of time-of-flight mass spectra. According to the calculations of Wada et al.,[32] the excitation spectrum of silver atoms embedded in helium droplets can be decomposed into three components. Consequently, the silver atoms have been excited at three different wavelengths corresponding approximately to the maxima in these distributions. The products are ionized by the 292.5 nm radiation from the second laser. Figure 2 shows the mass spectra in the range of 100−130 amu for silver atoms embedded in helium droplets with a mean radius of 37 Å. The mass spectrum resulting from excitation via the D1 transition at 332.5 nm is characterized by two intense peaks which are readily assigned to the two silver isotopes, ^{107}Ag and ^{109}Ag. The much weaker peaks at 111 and 113 amu correspond to the two AgHe isotopomers. Excitation via the D2 transitions at 322.5 and 315 nm leads to the formation of not only Ag and AgHe but also of appreciable amounts of $AgHe_2$. It should be noted that within the present signal-to-noise ratio we see no evidence of $AgHe_N$ exciplexes with $N > 2$ being formed. This in sharp contrast to the simulations by Wada et al.[32] that show the formation of $AgHe_N$ exciplexes with N up to 5.

Since the excitation spectra indicated that the formation efficiency is droplet size dependent, we have systematically recorded mass spectra for a wide range of droplet sizes. By integrating the area underneath each mass peak in the spectrum, it becomes possible to determine the relative abundance of each product with high accuracy. Figure 3 shows the relative abundances of AgHe and $AgHe_2$ as a function of droplet size for the three different excitation wavelengths. It should be mentioned that these relative abundances have been determined

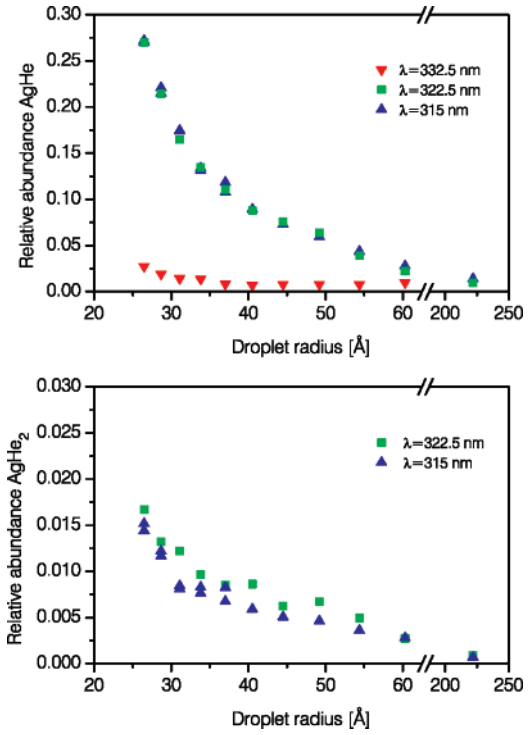

Figure 3. Upper panel: relative abundance of AgHe exciplexes following excitation at 332.5, 322.5, and 315 nm. Lower panel: relative abundance of $AgHe_2$ following excitation at 322.5 and 315 nm.

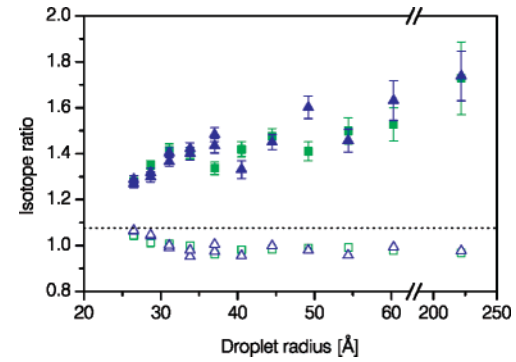

Figure 4. Isotope ratio of ^{107}Ag to ^{109}Ag (open symbols) and ^{107}AgHe to ^{109}AgHe exciplexes (closed symbols) ejected from the droplets following excitation at 322.5 (squares) and 315 nm (triangles). The dotted line indicates the natural isotope ratio.

by taking into account the signal of the two isotopes. The graph clearly demonstrates that the AgHe and $AgHe_2$ exciplexes are more efficiently formed at smaller droplet sizes. The apparent leveling off at larger droplet sizes for D1 excitation is caused by the contribution of the ionization laser to the signal.

A careful analysis of the time-of-flight mass spectrum reveals that the isotope ratio of the products does not reflect their natural abundance. Figure 4 shows the isotope ratio for the Ag and AgHe products as a function of mean droplet radius following excitation at $\lambda = 322.5$ nm and $\lambda = 315$ nm. The ^{107}Ag isotope appears to be depleted with respect to its natural abundance. In contrast, the ^{107}AgHe isotope is strongly enhanced. Both the depletion of ^{107}Ag and the enhancement of ^{107}AgHe show a noticeable droplet size dependence, indicating that these observations are not due to experimental conditions but are related to the dynamics taking place in the helium droplets. Based on these observations, it must be concluded that ^{107}Ag isotope is more efficiently converted into AgHe than the heavier ^{109}Ag isotope. The fact that a mass difference of only 5% gives rise

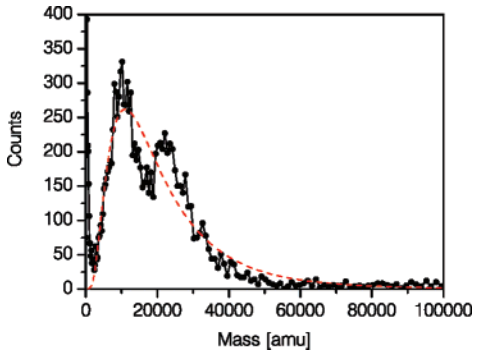

Figure 5. Time-of-flight mass spectra recorded following 310 nm excitation of silver atoms embedded in helium droplets consisting on average of 6000 helium atoms. The dotted line is a fit of the mass spectrum to a log-normal distribution.

to enhancement on the order of 25% strongly suggests that tunneling is involved in the formation of AgHe.

From the results presented above, it is obvious that a large fraction of the excited silver atoms is ejected from the droplets. However, it is well possible that some fraction of the excited silver remains solvated inside the droplets. The existence of such species is expected to show up in the time-of-flight mass spectrum at masses corresponding to the mass of the helium droplets, i.e., in the mass range of 10 000 amu. The time-of-flight mass spectrum recorded following 310 nm excitation of silver atoms embedded in helium droplets formed with a mean radius of 41 Å is reported in Figure 5. The mass spectrum reveals the presence of a weak signal in the high mass range. The signal is found to shift according to droplet size, indicating that the signal indeed originates from charged helium droplets. By monitoring the high mass signal as a function of oven temperature, i.e., the Ag vapor pressure, the possibility has been ruled out that the observed signal originates from the ionization of impurities picked up by the droplets. Although the mass spectrum is rather noisy, it can be reasonably well fitted to a log-normal distribution. The fit yields a mean mass of 22 000 amu, which corresponds to a droplet consisting of on average 5500 helium atoms. This value is close to the expected number of 6000 helium atoms for droplets produced under the present experimental conditions.[33,39] We can therefore safely state that the mass spectrum indicates that some fraction of the excited silver atoms remains attached to the droplets.

3.3. Photoelectron and ZEKE Spectra. The state resolved excitation spectra already provided details about the state distributions of the products. Complementary information can be obtained from photoelectron spectroscopy. Whereas normally photoelectron spectroscopy is used to investigate the energy levels of the ion, in the present experiments it is used to probe the state distribution of the ejected silver products. At the same time, photelectron spectroscopy might provide additional evidence for the solvation of excited silver atoms in the droplets. Photoelectron images have been recorded at the excitation wavelengths of 332.5 and 316 nm, corresponding to D1 and D2 excitations, respectively. To achieve the highest possible resolution, the wavelength of the ionization laser was set to 316 nm to create electrons with minimal energy. Figure 6 shows an electron image recorded at the excitation wavelength of 316 nm for droplets created with a mean radius of 41 Å. By applying an inverse Abel transformation to the image, the photoelectron spectrum can be obtained. The resulting photoelectron spectrum together with that obtained at the excitation wavelength of 332.5 nm is presented in Figure 7. The two photoelectron spectra are clearly very different. The spectrum resulting from excitation

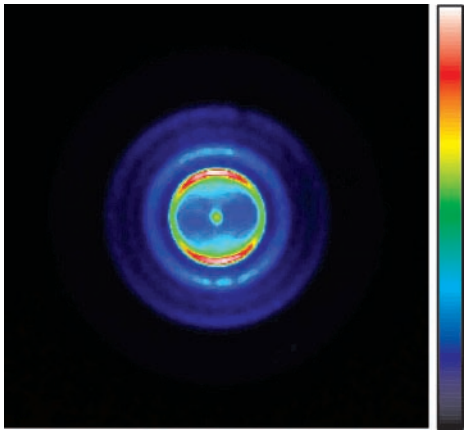

Figure 6. Photoelectron image recorded following 316 nm excitation of silver atoms embedded in helium droplet with a mean radius of 41 Å.

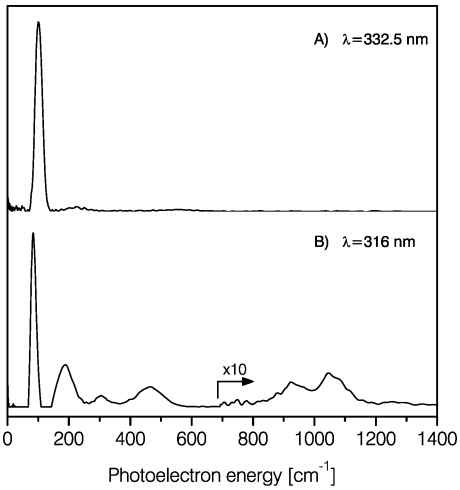

Figure 7. Photoelectron spectra derived from photoelectron images recorded following excitation of silver atoms at a wavelength of 332.5 (upper panel) and 316 nm (lower panel). The silver atoms are embedded in helium droplets with a mean radius of 41 Å.

via the D1 transition is dominated by a single peak, which can be unambiguously assigned to originate from Ag atoms in the $^2P_{1/2}$ state. In contrast, the photoelectron spectrum resulting from excitation via the D2 band consists of several peaks. The time-of-flight mass spectra have revealed that excitation via the D2 band leads to the ejection of not only silver atoms, but also AgHe and $AgHe_2$ exciplexes. In addition, a noticeable fraction of the excited silver atoms becomes solvated. Accordingly, the photoelectron spectrum is expected to reflect the presence of all these species. The peak corresponding to Ag $^2P_{1/2}$ is readily identified in the spectrum. The assignment of the other peaks is less obvious.

We will start our assignment of the photoelectron spectrum by identifying features in the spectrum that correspond to dissolved excited silver atoms. Recent photoelectron experiments on aniline embedded in helium nanodroplets have shown that the vertical ionization threshold of the aniline is lowered due to polarization effects and consequently depends on the droplet size.[40] To identify the presence of solvated excited silver atoms, we have therefore recorded photoelectron spectra for a series of different droplet sizes. Figure 8 shows the spectra obtained at three different droplet sizes. Inspection of the spectra reveals that the positions of the peaks at about 200 and 450 cm^{-1} vary with droplet size. The shift of these two peaks as a function of droplet size has been methodically determined. The results are

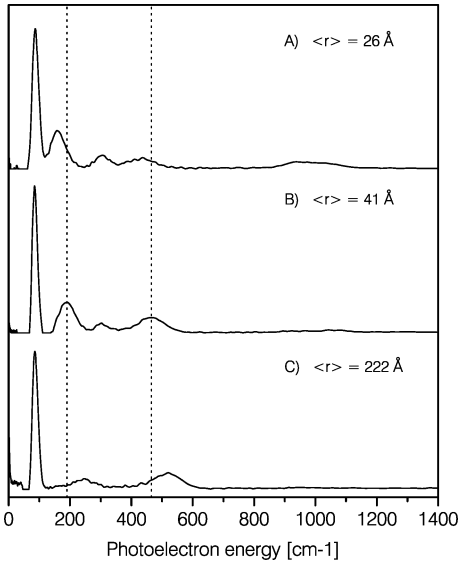

Figure 8. Photoelectron spectra derived from photoelectron images recorded following excitation of silver atoms at a wavelength of 316 nm. The silver atoms are embedded in helium droplets with mean radii of 26 (A), 41 (B), and 222 Å (C). The dotted lines are intended to facilitate the observation of peak shifts.

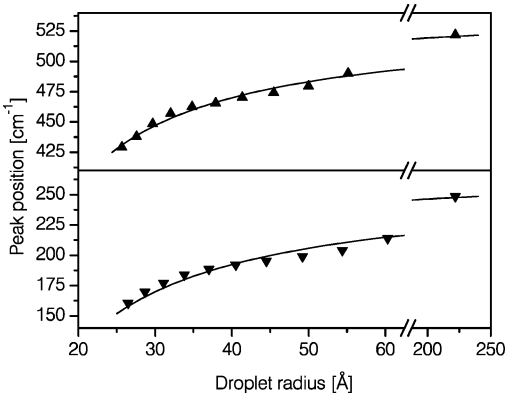

Figure 9. Variation of the peak positions of two selected transitions in the photoelectron spectrum with droplet size. The solid line is a fit of the data points to the functional form of eq 1.

plotted in Figure 9. Both peaks shift systematically to higher energy with increasing droplet size, which is consistent with a lowering of ionization threshold with increasing droplet size. It has recently been shown[40] that the vertical ionization threshold of embedded species varies with the droplet radius R according to

$$\mathrm{IP}(R) = \mathrm{IP}_\infty - \frac{e^2(1-\epsilon^{-1})}{8\pi\epsilon_0 R} \qquad (1)$$

where IP_∞ is the vertical ionization threshold in bulk helium, e is the electron charge, ϵ_0 is the permittivity of free space, and ϵ is the dielectric constant of the cluster. Under the assumption that the energy of the dissolved excited silver atoms does not depend on droplet size, the peak positions in the photoelectron spectra should show the same R dependence as the ionization threshold. Consequently, the peak positions have been fitted to this functional form. The constant found describing the R dependence is with 2600 cm^{-1}/Å relatively close the theoretically predicted value. This together with the fact that the width of these peaks is significantly broader than the instrumental resolution is taken as evidence that both these peaks correspond to dissolved excited silver atoms. Based on the relative

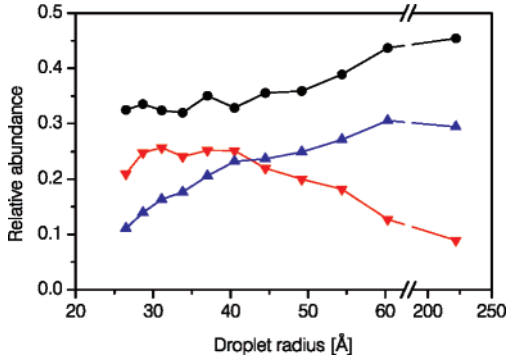

Figure 10. Relative abundance of Ag $^2P_{1/2}$ (●) and of dissolved silver atoms characterized by the peaks in the photoelectron spectrum at 200 (▼) and 450 cm^{-1} (▲). The lines through the data points are to guide the eye.

intensities of these two peaks in the photoelectron spectrum, one must conclude that roughly half of the D2 excited silver atoms become dissolved by the helium. By integrating the area underneath each peak in the photoelectron spectrum, it becomes possible to determine accurately the relative contribution of each product. The results for different droplet sizes are plotted in Figure 10. As can be inferred from this figure, the relative intensity of the peaks varies weakly with droplet size. While the peak at 450 cm^{-1} gains intensity with increasing droplet size, the intensity of the peak at 200 cm^{-1} decreases with increasing droplet size.

The photoelectron images not only yield the kinetic energy of the electrons; they also provide information on the angular distribution of the electrons. Inspection of the electron image shown in Figure 6 immediately reveals that the angular distributions of the electrons originating from Ag $^2P_{1/2}$ and dissolved silver atoms are quite similar. A more quantitative analysis of the image shows that all three angular distributions are well described by an anisotropy parameter of $\beta = 0.45$. As we will show below, this information can be used to determine the character of the dissolved silver atoms.

Having assigned these two peaks in the spectrum to dissolved silver atoms, the other peaks have to be attributed to $^2P_{3/2}$ Ag and AgHe and possibly $AgHe_2$. The spin−orbit splitting of the excited silver atoms is well-known to equal 920.6 cm^{-1}.[41] Consequently, the peak in the photoelectron spectrum at around 950 cm^{-1} can be attributed to $^2P_{3/2}$ Ag. However, the width of this peak as well as that at 1050 cm^{-1} is substantially broader than the experimental resolution, indicating that several transitions contribute to it. Attempts to resolve the transitions by reducing the kinetic energy of the corresponding photoelectrons were not successful. Therefore, it was decided to use a ZEKE detection scheme, which allows recording spectra with much higher resolution.

The experimental conditions used to perform ZEKE spectroscopy have been described in detail in the experimental section. Since spectra with a sufficient signal-to-noise ratio could not be obtained in a two-laser experiment due to the nonoptimal spatial and temporal overlap of the laser beams, the experiments have been carried out using a single laser. This laser beam excites the silver atoms in the helium droplets and subsequently excites the products to high Rydberg levels, which are subsequently probed by the ZEKE detection scheme. The use of a single laser implies that the intensities in the ZEKE spectrum will be convoluted by the absorption spectrum of the embedded silver atoms. In addition, the intensities in the ZEKE spectrum will depend on the species being probed since the lifetimes of Rydberg states in molecular systems are generally affected by

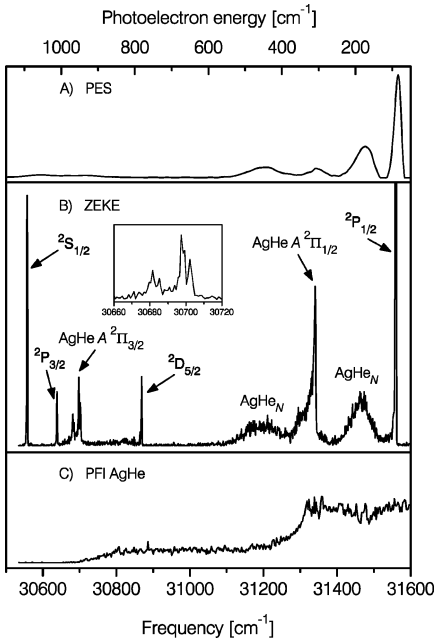

Figure 11. One-color ZEKE spectrum of silver atoms embedded in helium droplets with a mean radius of 31 Å (middle panel) and corresponding photoelectron spectrum (upper panel). The inset in the middle panel shows a detailed view of that part of the spectrum that corresponds to transitions involving AgHe $A^2\Pi_{3/2}$. The lower panel shows the field-free AgHe ion yield spectrum recorded using pulsed field ionization for the detection of AgHe ions.

nonradiative processes.[42] Figure 11 shows the ZEKE spectrum and the corresponding photoelectron spectrum resulting from the excitation of silver atoms in helium droplets with a mean radius of 31 Å. The high-resolution ZEKE spectrum reveals that the peaks around 1000 cm^{-1} in the photoelectron spectrum consist of several individual lines. The sharp lines in the ZEKE spectrum can be readily assigned to transitions belonging to free silver atom. The line at 30 553 cm^{-1} corresponds to ZEKE detection of ground state silver atoms via two-photon excitation.[43] The origin of this signal will be discussed below. It is straightforward to assign the sharp lines at 31 555, 30 634, and 30 864 cm^{-1} to transitions originating from the $^2P_{1/2}$, $^2P_{3/2}$, and $^2D_{5/2}$ states of silver, respectively.[41,43] The ZEKE spectrum thus convincingly demonstrates that silver atoms in the $^2D_{5/2}$ state are formed and that at least some fraction is ejected from the droplets. The broad peaks in the ZEKE spectrum around 31 150 and 31 450 cm^{-1} correspond to transitions of the dissolved excited helium atoms. These lines could be accurately fitted to a Gaussian distribution. The peak positions show the same droplet size dependence as observed in the photoelectron spectrum. The widths of the peaks could be accurately determined from the ZEKE spectra and were found to be almost independent of droplet size and to equal 110 and 55 cm^{-1} fwhm for the peaks at 31 150 and 31 450 cm^{-1}, respectively.

Having assigned most of the peaks in the spectrum to either gas-phase or dissolved silver atoms, the remaining features in the ZEKE spectrum have to be attributed to AgHe and $AgHe_2$. Since the time-of-flight mass spectra indicate that AgHe is the most abundant product after Ag, it seems logical to assign the broad structures at 30 700 and 31 340 cm^{-1} to AgHe. To verify the assignment, we have attempted to record MATI spectra for AgHe and $AgHe_2$, but without success. Although this could indicate that these peaks in the ZEKE spectrum do not originate from AgHe, it is more likely that at the voltage settings used for MATI detection, which are considerably different from those used for ZEKE, the excited Rydberg states of AgHe decay

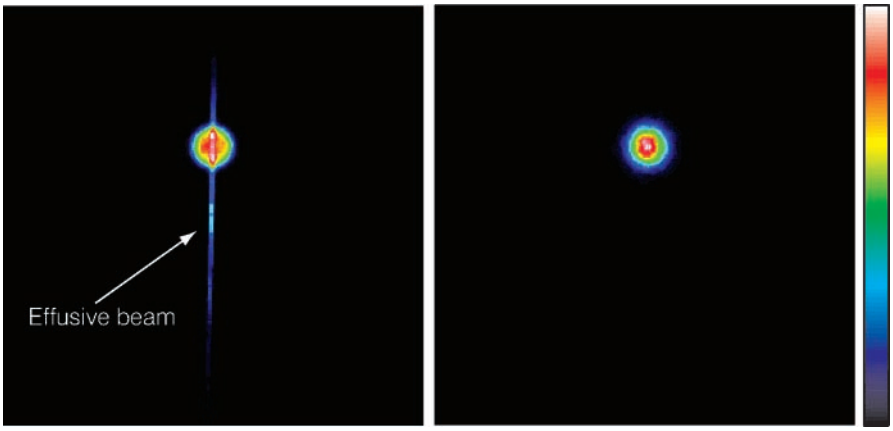

Figure 12. Ion images corresponding to silver atoms in the ground state (left) and $^2P_{1/2}$ state (right). The images are recorded following excitation of silver atoms embedded in helium droplets with a mean radius of 60 Å.

before they are field ionized. To confirm this, we have recorded an AgHe ion yield spectrum under field-free conditions using pulsed field extraction for the detection of the ions. The resulting spectrum is displayed in Figure 11. The steps in the ionization yield clearly coincide with the two unassigned peaks in the ZEKE spectrum. Consequently, the lines around 30 700 and 31 340 cm^{-1} in the ZEKE spectrum are assigned to AgHe.

3.4. Ion Imaging. The ZEKE spectra revealed the presence of ground state silver atoms. These atoms can originate from several different sources or processes. Silver atoms that have been transported into the detection region by the effusive beam that emerges from the oven will certainly contribute to the detected signal. Another contribution might come from excited silver atoms ejected from the droplets that have decayed radiatively to the ground state during the 5 ns laser pulse. In view of the 7.4 ns lifetime of the 5p states of silver,[44] this fraction can be significant. Another contribution could possibly originate from the nonradiative relaxation of dissolved electronically excited silver atoms. Spectroscopic studies on optically excited alkali metal atoms in bulk liquid helium indicate that this process is the main relaxation pathway for the light alkali metals Li, Na, and K.[45,46] The excess energy of approximately 30 000 cm^{-1} that will be released in this process will be sufficient to completely evaporate all but the largest droplets and thus yield free ground state silver atoms. Based on the ZEKE spectrum it is not possible to disentangle these various contributions. However, more can be learned about the contribution of the various processes by using quantum-state-specific ion imaging since the speed distributions of the silver atoms will depend on the formation process. Figure 12 shows two ion images recorded under identical experimental conditions. The left image corresponds to ground state silver atoms while the one on the right corresponds to Ag $^2P_{1/2}$ atoms. The images are clearly not identical, indicating that different processes give rise to these products. The image corresponding to ground state silver atoms shows an easily recognizable vertical streak that is substantially displaced with respect to the origin of the setup. This feature can be attributed to silver atoms in the effusive beam emerging from the oven since these atoms have a highly anisotropic velocity distribution. In addition to the effusive beam structure, an isotropic signal is observed. Based on the characteristic displacement on the detector, this structure is readily identified as ground state silver atoms originating from the droplets. The speed distribution of these ground state atoms is identical to that of the electronically excited $^2P_{1/2}$ silver atoms shown in the right image. This strongly suggests that these ground state atoms result from $^2P_{1/2}$ silver atoms ejected from the droplets that have decayed during the 5 ns laser pulse. Although it cannot be completely ruled out that nonradiative relaxation of excited silver atoms to the ground state ground occurs, the present results do indicate that this mechanism does not play an important role in the excited state dynamics of silver atoms in helium droplets.

4. Discussion

Having presented all the available data, we are now in the position to discuss in more detail the excited state dynamics of silver atoms embedded in helium droplets. All the excitation spectra reported in this work show that the absorption bands corresponding to the D1 and D2 transitions are fully separated and thus do not partially overlap. This is clearly at odds with the absorption spectra calculated by both diffusion Monte Carlo and path integral Monte Carlo methods, which both show an appreciable overlap of the two bands.[31,32] It could be argued that the excitation spectra recorded in the present work do not truly reflect the absorption spectrum. Indeed, the photoelectron spectra reveal that following excitation via the D2 band a significant fraction of the excited atoms becomes dissolved in the helium droplets. The detection efficiency of these dissolved species is substantially less than that of Ag and AgHe. Accordingly, the recorded excitation spectrum does not necessarily reflect the absorption spectrum. On the other hand, the bands in the excitation spectra of the Ag and AgHe products, which probably result from different formation processes, have identical shapes. In addition, the laser induced fluorescence spectra of silver atoms in bulk helium clearly reveal that the two bands are fully separated.[27] In view of this we argue that the spectra recorded in this work are representative of the absorption spectrum of helium-embedded silver atoms. It is important to realize that this could have consequences for models that have been proposed to account for the efficient $^2P_{1/2} \leftarrow {}^2P_{3/2}$ relaxation. Based on the partial overlap of the D1 and D2 bands, Mella et al. suggested that the coupling between the states corresponding to these bands could account for the observed relaxation.[31] However, this process is expected to be considerably less efficient in case the bands do not overlap, and consequently is most likely not responsible for the efficient relaxation.

The quantum molecular dynamics simulations by Wada et al. indicate that the excited state dynamics is mainly governed by nonadiabatic transitions between the various potential energy surfaces.[32] Their simulations reveal that the population of the silver atoms following excitation is almost equally distributed

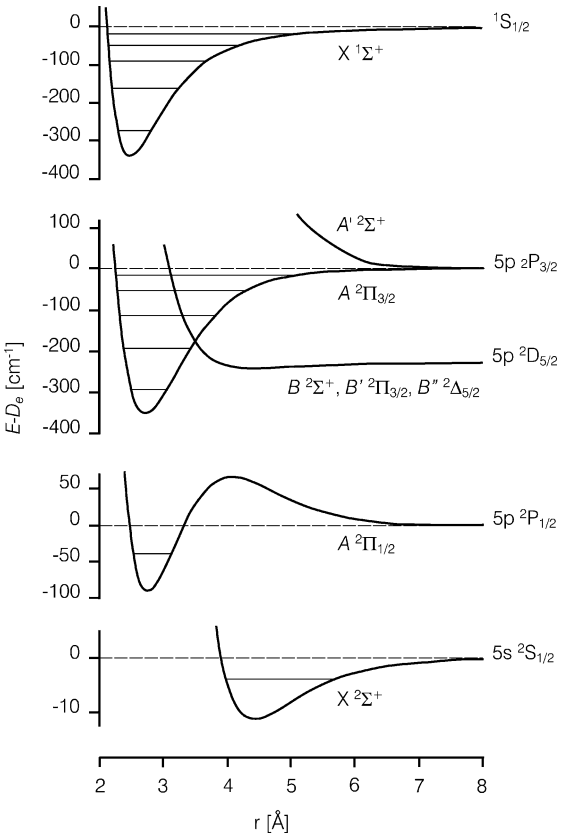

Figure 13. Potential energy curves of the ground state of $AgHe^+$ and the lowest electronic states of AgHe. The curves for AgHe are taken from ref 47.

over the $^2P_{1/2}$ and $^2P_{3/2}$ states, independent of the state initially populated. These results are in strong contrast to what has been observed experimentally. The photoelectron spectra namely reveal that excitation via the D1 band yields almost exclusively Ag $^2P_{1/2}$ atoms. In contrast, excitation via the D2 band not only yields free Ag $^2P_{1/2}$ atoms, but also yields an appreciable amount of $^2P_{3/2}$ silver atoms. These observations signify that nonadiabatic transitions alone cannot be responsible for the observed state distributions. It thus becomes apparent that other mechanisms that have not been taken into account in the simulations play a more important role in determining the state populations.

One of the important aspects not included in the simulations is the presence of the intermediate metastable $^2D_{5/2}$ state. Although direct excitation to this state is optically forbidden, it could play an important role in the relaxation of $^2P_{3/2}$ excited silver atoms. The experiments by Takami and co-workers on the radiative lifetime of silver atoms in dense helium gas seem to confirm the importance of this state in the relaxation process.[28] They found that the radiative lifetime of Ag $^2P_{1/2}$ atoms formed by excitation to the $^2P_{3/2}$ level exceeds by far that of free silver atoms. Based on this observation the authors concluded that the $^2P_{3/2} \rightarrow {}^2P_{1/2}$ relaxation mechanism must proceed via the intermediate metastable $^2D_{5/2}$ state. In addition, when increasing the helium density, they noticed a rather abrupt shortening of the lifetime and a striking change in the relative intensities of the Ag $^2P_{1/2}$ and $AgHe_2$ fluorescence. The mechanism responsible for these observations could be deduced with the help of ab initio potential energy curves of the AgHe complex.[47] These curves are partially reproduced in Figure 13 to facilitate the discussion of the proposed mechanism. The authors argued that, following excitation of silver atoms via the D2 band in dense helium gas, AgHe complexes readily form in the $A^2\Pi_{3/2}$ state. A substantial fraction of the vibrationally excited AgHe subsequently predissociates to form metastable $^2D_{5/2}$ silver atoms, while another fraction will bind one more helium atom to form $AgHe_2$ in the $^2\Pi_{3/2}$ excited state. Due to the weak attractive forces between the $^2D_{5/2}$ Ag and the helium atoms, a shell of helium atoms will form around the metastable silver atom. The authors showed that above a critical helium density the electronic states correlating to $^2P_{1/2}$ silver atoms will cross the states correlating to the $^2D_{5/2}$ state. This curve crossing is then responsible for the transfer of population from the $^2D_{5/2}$ to the $^2P_{1/2}$ state. The internuclear distance at which the curve crossing is estimated to occur, $r_{cc} = 4.5$ Å, is somewhat larger than the position of the potential barrier, $r_b = 4.09$ Å, in the $A^2\Pi_{1/2}$ state AgHe; see Figure 13. Consequently, the curve crossing should yield exclusively $^2P_{1/2}$ Ag atoms as the formation of AgHe $^2\Pi_{1/2}$ is inhibited by the potential barrier. This barrier in the AgHe $^2\Pi_{1/2}$ potential is also thought to inhibit the formation of AgHe and $AgHe_2$ following optical excitation via the D1 transition. In conclusion, the relaxation mechanism proposed by Takami and co-workers is thought to produce exclusively silver atoms in the $^2P_{1/2}$ state and $AgHe_2$ in the $^2\Pi_{3/2}$ electronic state.

As we will show now, the results of the present study provide additional support for this relaxation mechanism but at the same time also point out some shortcomings. If the $^2D_{5/2}$ state plays a key role in the relaxation of silver atoms excited to the $^2P_{3/2}$ state, it should be possible to detect silver atoms in this quantum state. Indeed, the ZEKE spectrum recorded in this study reveals a relatively weak transition at 30 864 cm^{-1} that could be unambiguously assigned to originate from silver atoms populating the $^2D_{5/2}$ state. Although this does not prove the existence of the mechanism proposed by Takami and co-workers,[28] it does support it. Additional support is provided by the time-of-flight mass spectra, which reveal the formation of AgHe following excitation via the D2 transition. In contrast to the predictions made by the model, the ZEKE and pulsed field ionization spectra unmistakably reveal the formation of AgHe populating not only the $^2\Pi_{3/2}$ state but also the $^2\Pi_{1/2}$ state. In fact, the photoelectron spectra indicate that the majority of the AgHe leaving the droplets resides in the $^2\Pi_{1/2}$ state and not the $^2\Pi_{3/2}$ state. This observation at first might seem to contradict the model. However, it should be noted that the barrier in the $AgHe^2\Pi_{1/2}$ potential is relatively small and that the curve crossing occurs relatively close to the top of the barrier. It is therefore well possible that the formation of AgHe occurs by tunneling through this barrier. Tunneling has also been thought to be responsible for the formation of alkali metal−helium complexes after optical excitation of alkali metal atoms located on the surface of helium droplets.[48,49] Supporting evidence that tunneling is involved in the AgHe formation is given by the time-of-flight mass spectra. These spectra show that following D2 excitation the isotope ratio of AgHe deviates substantially from the natural Ag abundance. The lighter ^{107}AgHe complex is 25% more abundant than the heavier isotopomer while at the same time the bare ^{107}Ag isotope appears to be depleted; see Figure 4. This huge isotope effect clearly points to a tunneling process. It should be realized that the fact that mainly AgHe products in the $^2\Pi_{1/2}$ state are detected does not imply that the majority is formed in this state. The ejection dynamics could be different for these two electronic states. It is interesting to note that the quantum Monte Carlo simulations by Wada et al. that do not include the metastable $^2D_{5/2}$ state of silver find that the $AgHe_N$ exciplexes are mainly formed in electronic states correlating with the $^2P_{1/2}$ state of the free silver atom.[32]

TABLE 1: Calculated Energies and Rotational Constants of Vibrational Levels of the $X^1\Sigma^+$ Ground State of the $AgHe^+$ Ion and $A^2\Pi_{3/2}$ Electronically Excited State of AgHe

	$AgHe^+$ $X^1\Sigma^+$		AgHe $A^2\Pi_{3/2}$[a]	
v	$E_v - D_e$ [cm^{-1}]	B_v [cm^{-1}]	$E_v - D_e$ [cm^{-1}]	B_v [cm^{-1}]
0	−273.8	0.676	−293.3	0.563
1	−166.1	0.580	−192.8	0.507
2	−90.1	0.475	−112.0	0.443
3	−41.9	0.361	−52.3	0.367
4	−15.9	0.247	−14.9	0.267

[a] Reference 47.

The photoelectron spectrum following D2 excitation reveals two broad structures, in addition to the peaks corresponding to Ag and AgHe. Based on the variation of the position of these peaks with droplet size, it is concluded that these structures correspond to excited silver atoms dissolved in the helium droplets. These structures are also present in the photoelectron spectra for large helium droplets containing millions of helium atoms, which are representative for bulk helium. It thus appears justified to follow Takami and co-workers[27] and assign one of the peaks to $AgHe_2$ $^2\Pi_{3/2}$ ($v = 0$). The laser induced fluorescence spectra of photoexcited silver atoms rule out the presence of dissolved AgHe or vibrationally excited $AgHe_2$ $^2\Pi_{3/2}$.[27] Consequently, the other broad structure in the photoelectron spectrum is not likely to originate from any of these products. More information about the character of the dissolved silver atoms can be inferred from the angular distributions of the photoelectrons. The angular distributions of the peaks in the photoelectron spectrum that correspond to dissolved silver atoms are both characterized by an anisotropy parameter of 0.45. This indicates that the states have the same symmetry, which rules out that one of the peaks found in the photoelectron spectrum originates from silver atoms in the metastable $^2D_{5/2}$ state. Takami and co-workers concluded that only $AgHe_2$ in the $\tilde{A}^2\Pi_{3/2}$ state can be formed since the presence of a barrier in the potential energy curve of the $\tilde{A}^2\Pi_{1/2}$ state inhibits the formation of $AgHe_2$ in this state. On the other hand, the detection of AgHe in the $^2\Pi_{1/2}$ state indicates that the barrier does not completely impede the formation of AgHe in this state. Consequently, it seems not unreasonable to assign the other broad peak in the photoelectron spectrum to $AgHe_2$ $\tilde{A}^2\Pi_{1/2}$ ($v = 0$). This assignment is compatible with the laser induced fluorescence spectrum as recorded by Persson et al.[27] if it is assumed that the fluorescence spectrum resulting from the $^2\Pi_{1/2}$ state is similar to that of the $^2\Pi_{3/2}$ state but shifted by the spin−orbit splitting. In addition, the formation of $AgHe_2$ in the $^2\Pi_{1/2}$ state could also account for a seemingly contradicting observation in the experiments on silver atoms in dense helium gas. In the study of Jakubek et al.[28] the abrupt change in radiative lifetime with increasing density was accompanied by a change in the relative fluorescence intensity of Ag $^2P_{1/2}$ and $AgHe_2$. While the radiative lifetime decreased by a factor of 20, the relative fluorescence ratio changed only by a factor of 6. This does not appear to be consistent with the proposed model. However, if $AgHe_2$ is also formed in the $^2\Pi_{1/2}$ state, this observation can be accounted for.

Having assigned the broad structures in the photoelectron spectrum to $AgHe_2$ in $^2\Pi_{3/2}$ ($v = 0$) and $^2\Pi_{1/2}$ ($v = 0$), we can now attempt to estimate the energies of these states. However, before doing so we would like to discuss the energy levels of AgHe in more detail since these electronic states appear to play a crucial role in the excited state dynamics. In the present study, information about the energy levels of AgHe can only be obtained from the ZEKE spectra. The resolution in the present study is not sufficient to resolve individual rovibronic transitions, and therefore the amount of information that can be extracted from the spectra is limited. However, there is a clear difference between the spectroscopic features corresponding to the $^2\Pi_{1/2}$ and $^2\Pi_{3/2}$ states. While the former consists of a single sharp line residing on a broad background, the latter consists of two doublets (doublet splitting ~4 cm^{-1}) that are separated by approximately 17 cm^{-1}. This spectral difference is probably related to the internal energy distribution of AgHe in the two electronic states involved. The ab initio calculations by Jakubek and Takami indicate that the $^2\Pi_{1/2}$ state can hold only a single vibrational level while the $^2\Pi_{3/2}$ state can support five vibrational levels.[47] In addition, the $^2\Pi_{3/2}$ state also supports many more rotational levels than the $^2\Pi_{1/2}$ state. Furthermore, it was found that the repulsive part of the electronic states that correlate to Ag $^2D_{5/2}$ cross the $^2\Pi_{3/2}$ state at an energy just above the $v = 1$ level. According to the mechanism proposed by Takami, only the $v = 0$ and $v = 1$ levels of the $^2\Pi_{3/2}$ state of AgHe will be significantly populated. To determine whether the observed spectral features are consistent with this model, it is necessary to know the energy levels of the $AgHe^+$ ion. We therefore have calculated the potential energy curve of the $AgHe^+$ ion by ab initio methods using the Gaussian 03 package.[50] The potential energy curve has been calculated at the CCSD(T) level of theory and has been corrected for the superposition error using the counterpoise correction procedure by Boys and Bernardi.[51] To be consistent with the calculations of Jakubek and Takami on AgHe, we have used the same set of basis functions as these authors.[47] The potential energy curve for $AgHe^+$, depicted in Figure 13, exhibits a minimum of 340.5 cm^{-1} at an internuclear distance of 2.46 Å and, hence, is rather similar to that of the $^2\Pi_{3/2}$ state of AgHe. Accordingly, the Franck−Condon principle will favor $\Delta v = 0$ transitions for the $X^1\Sigma^+$ $AgHe^+ \leftarrow A^2\Pi_{3/2}$ AgHe system. The energies and rotational constants of the vibrational levels of $AgHe^+$ have been calculated by numerically solving the Schrödinger equation[52] and are reported in Table 1. Using these values, the splitting between the $v' = 0 \leftarrow v'' = 0$ and $v' = 1 \leftarrow v'' = 1$ transitions is calculated to equal 7.2 cm^{-1}. Since the electron created in the ionization process can carry away orbital angular momentum, the change in the rotational angular momentum of AgHe is not limited to the usual $\Delta N = 0, \pm 1$ selection rule; also larger values are allowed. This can lead to the formation of multiple band heads in the ZEKE spectrum. Based on the computed rotational constants, the splitting between the band heads is expected to be on the order of 10 cm^{-1}. In view of the accuracy of the calculated energy levels and rotational constants, one can conclude that the ZEKE spectrum is compatible with transitions originating from the $v = 0$ and $v = 1$ levels of AgHe in the $A^2\Pi_{3/2}$ state. Having established the character of the transitions in the spectrum, it now becomes possible to determine the spin−orbit splitting for the excited states of AgHe. From the ZEKE spectrum, we deduce a splitting of approximately 640 cm^{-1}. This value is slightly larger than the theoretical value of 614 cm^{-1} that is based on the assumption that the spin−orbit interaction in AgHe

is independent of the internuclear distance and therefore equals 2/3 the spin−orbit splitting in the silver atom. However, if the zero point energies of the $^2\Pi_{3/2}$ and $^2\Pi_{3/2}$ curves are taken into account, the calculated splitting is with 666 cm^{-1} only slightly larger than the observed splitting.[32] Under the assumption that the ab initio calculations yield the correct dissociation limit for $AgHe^+$, it becomes possible to calculate the binding energies for both the $^2\Pi_{1/2}$ state and the $^2\Pi_{3/2}$ state. From the observed transition frequencies in the ZEKE spectrum and the calculated energy levels of the $AgHe^+$ ion, we find binding energies of 55 and 335 cm^{-1} for the $v = 0$ level of the $^2\Pi_{1/2}$ state and $^2\Pi_{3/2}$ state, respectively. These values compare very favorably with the energies of 39 and 293 cm^{-1} calculated by Jakubek and Takami.[47]

We can now return to the broad structures in the photoelectron and ZEKE spectra that are thought to arise from dissolved $AgHe_2$ in the $^2\Pi_{1/2}$ and $^2\Pi_{3/2}$ states. Before we discuss the energies of these states, we first have to assign the two bands. Based on the observations for AgHe, it appears reasonable to assign the highest energy state, corresponding to the peak at 31 150 cm^{-1} in the ZEKE spectrum, to $AgHe_2$ $\tilde{A}^2\Pi_{3/2}$. Since recent photoelectron experiments have shown that the vibrational relaxation of molecules in helium droplets is complete on a nanosecond time scale,[40] it is safe to assume that both peaks in the photoelectron spectrum and ZEKE spectrum probe the ground state configuration. If the splitting between the states in the ZEKE spectrum is taken as the spin−orbit splitting between the states, one arrives at a value of 280 ± 5 cm^{-1}. This value is approximately a factor of 2 less than what would be expected based on the assumption that the spin−orbit interaction in $AgHe_N$ is independent of the internuclear distance. The reduced splitting could thus signify that while this approximation is valid for AgHe it is no longer appropriate for large $AgHe_N$ complexes. However, when interpreting the ZEKE and photoelectron spectra, one should take into account that both these detection schemes probe the vertical ionization threshold. When a positively charged ion is embedded in liquid helium, it forms a compact solvation structure which is often referred to as a snowball.[53] The solvation structures formed around neutral species are in general very different from those formed around ions.[31] As a result, the ionization of dissolved excited silver will probe not the adiabatic ionization threshold but rather the corresponding vertical thresholds. The ab initio calculations by Persson et al. for $AgHe_2$ indicate that the equilibrium structures for both spin−orbit states are almost identical but that the binding energies are very different.[27] It therefore is conceivable that the solvation structures of the $AgHe_2$ complexes in the droplets are not identical and consequently the vertical ionization thresholds could be different. The possible difference in solvation structure could thus account for the unexpected small splitting observed in the photoelectron and ZEKE spectra. At the same time, the difference in solvation structure could also give rise to a difference in line widths of the two bands. However, as the solvation structures of the species involved are not known, it is not possible to draw any further conclusions from these line widths.

Even though the photoelectron and ZEKE spectra do not allow us to probe the adiabatic ionization threshold, we can still use them to make a rough estimate of the solvation energies of the dissolved excited silver atoms. Our recent study on the photoelectron spectroscopy of aniline has shown that the vertical ionization threshold of dissolved aniline could be calculated by ab initio methods using the continuum model to within 200 cm^{-1}.[40] Assuming that a similar accuracy can be obtained for atomic ions, we have calculated the vertical ionization threshold for the silver atom. These calculations where performed at the CCSD(T) level of theory, while the interaction with the helium environment was taken into account using the continuum model initially devised by Tomasi and co-workers.[54] As before, the same basis sets of Jakubek and Takami have been used.[47] The calculations reveal that the ionization threshold is lowered by approximately 2100 cm^{-1} upon solvation by helium. By taking into account the variation of the ionization threshold with droplet size, the solvation energies of the excited silver atoms can be calculated from the observed transition frequencies. We find solvation energies of 1900 and 2500 cm^{-1} for the $^2P_{1/2}$ and $^2P_{3/2}$ states of silver, respectively. It should be stressed that these values are determined assuming that both states probe the same ionization threshold, something that is not necessarily true as we pointed out above. Moreover, it is assumed that silver atoms are dissolved in the helium droplets and not the proposed $AgHe_2$ exciplexes. Nevertheless, it is obvious that the solvation energies of excited silver atoms are much larger than that of ground state silver which has been calculated to be on the order of 100 cm^{-1}.[31]

The last issue we want to address is the droplet size dependence of the excited state dynamics. The time-of-flight mass spectra and photoelectron spectra have demonstrated that the yield of ejected AgHe $A^2\Pi_{1/2}$ exciplexes decreases monotonically with increasing helium droplet size. At the same time, the photoelectron spectra show that the relative amount of dissolved $AgHe_2$ $^2\Pi_{1/2}$ decreases with droplet size, while the relative amount of dissolved $AgHe_2$ $^2\Pi_{3/2}$ increases. Whereas the ejection process could account for the decrease of AgHe $^2\Pi_{1/2}$ exciplexes, at the same time it cannot be responsible for the reduction of solvated $AgHe_2$ $^2\Pi_{1/2}$. One therefore must conclude that the formation process of both these species is droplet size dependent.

5. Conclusion

The excited state dynamics of silver atoms embedded in helium nanodroplets have been investigated by a variety of spectroscopic techniques. The experiments reveal that excitation via the Dl transition results mainly in the ejection of $^2P_{1/2}$ excited silver atoms. In contrast, excitation to the $^2P_{3/2}$ state leads to the ejection of not only silver atoms in the $^2P_{1/2}$, $^2P_{3/2}$, and $^2D_{5/2}$ excited states but also of AgHe and $AgHe_2$. The AgHe exciplexes are mainly formed in the $A^2\Pi_{1/2}$ electronic state. The experiments furthermore show that following D2 excitation a considerable fraction of the excited silver atoms remains inside the helium droplet. Based on the photoelectron and ZEKE spectra recorded in the present study and the laser induced fluorescence spectra of silver in bulk helium recorded by Persson et al.,[27] it is concluded that the excited silver atoms become solvated as $AgHe_2$. These dissolved exciplexes are thought to form in the $\tilde{A}^2\Pi_{3/2}$ and $\tilde{A}^2\Pi_{1/2}$ excited states.

The experiments show that nonadiabatic transitions between the various potential curves as suggested by the quantum mechanical molecular dynamics simulations by Wada et al.[32] cannot be solely responsible for the observed product and state distributions. The detection of silver atoms in the metastable $^2D_{5/2}$ state appears to supports the model put forward by Takami and co-workers in which the $^2D_{5/2}$ state acts as a doorway state for the formation of Ag $^2P_{1/2}$.[28] Although some of the observations do not follow directly from the model, they can be readily brought into accord with this model. Hence, this study clearly demonstrates that any simulation that attempts to describe the excited state and translational dynamics of silver atoms in helium nanodroplets must take into account the $^2D_{5/2}$ state.

Acknowledgment. This research was made possible by the financial support of the Swiss National Science Foundation through Grant 200020-112193.

References and Notes

(1) Toennies, J. P.; Vilesov, A. F. *Annu. Rev. Phys. Chem.* **1998**, *49*, 1.
(2) Toennies, J. P.; Vilesov, A. F. *Angew. Chem., Int. Ed.* **2004**, *43*, 2622.
(3) Stienkemeier, F.; Vilesov, A. F. *J. Chem. Phys.* **2001**, *115*, 10119.
(4) Stienkemeier, F.; Lehmann, K. K. *J. Phys. B: At. Mol. Opt. Phys.* **2006**, *39*, R127.
(5) Kwon, Y.; Huang, P.; Patel, M. V.; Blume, D.; Whaley, K. B. *J. Chem. Phys.* **2000**, *113*, 6469.
(6) Barranco, M.; Guardiola, R.; Hernandez, S.; Mayol, R.; Navarro, J.; Pi, M. *J. Low Temp. Phys.* **2006**, *142*, 1.
(7) Choi, M. Y.; Douberly, G. E.; Falconer, T. M.; Lewis, W. K.; Lindsay, C. M.; Merritt, J. M.; Stiles, P. L.; Miller, R. E. *Int. Rev. Phys. Chem.* **2006**, *25*, 15.
(8) Rudic, S.; Merritt, J. M.; Miller, R. E. *J. Chem. Phys.* **2006**, *124*, 104305.
(9) Merritt, J. M.; Rudic, S.; Miller, R. E. *J. Chem. Phys.* **2006**, *124*, 084301.
(10) Merritt, J. M.; Kupper, J.; Miller, R. E. *Phys. Chem. Chem. Phys.* **2005**, *7*, 67.
(11) Nauta, K.; Miller, R. E. *Science* **1999**, *283*, 1895.
(12) Farnik, M.; Toennies, J. P. *J. Chem. Phys.* **2005**, *122*, 014307.
(13) Lewis, W. K.; Bemish, R. J.; Miller, R. E. *J. Chem. Phys.* **2005**, *123*, 141103.
(14) Peterka, D. S.; Kim, J. H.; Wang, C. C.; Neumark, D. M. *J. Phys. Chem. B* **2006**, *110*, 19945.
(15) Lewis, W. K.; Lindsay, C. M.; Bemish, R. J.; Miller, R. E. *J. Am. Chem. Soc.* **2005**, *127*, 7235.
(16) Yang, S. F.; Brereton, S. M.; Wheeler, M. D.; Ellis, A. M. *Phys. Chem. Chem. Phys.* **2005**, *7*, 4082.
(17) Braun, A.; Drabbels, M. *Phys. Rev. Lett.* **2004**, *93*, 253401.
(18) Braun, A.; Drabbels, M. Submitted for publication.
(19) Stolyarov, D.; Polyakova, E.; Wittig, C. *J. Phys. Chem. A* **2004**, *108*, 9841.
(20) Takayanagi, T.; Shiga, M. *Chem. Phys. Lett.* **2003**, *372*, 90.
(21) Landau, L. *J. Phys. USSR* **1941**, *5*, 71.
(22) Stienkemeier, F.; Higgins, J.; Ernst, W. E.; Scoles, G. *Phys. Rev. Lett.* **1995**, *74*, 3592.
(23) Hui, Q.; Persson, J. L.; Beijersbergen, J. H. M.; Takami, M. *Z. Phys. B* **1995**, *98*, 353.
(24) Bauer, H.; Beau, M.; Friedl, B.; Marchand, C.; Miltner, K.; Reyher, H. J. *Phys. Lett. A* **1990**, *146*, 134.
(25) Beijersbergen, J. H. M.; Qin, H.; Takami, M. *Phys. Lett. A* **1993**, *181*, 393.
(26) Kanorsky, S. I.; Arndt, M.; Dziewior, R.; Weis, A.; Hansch, T. W. *Phys. Rev. B* **1994**, *50*, 6296.
(27) Persson, J. L.; Hui, Q.; Jakubek, Z. J.; Nakamura, M.; Takami, M. *Phys. Rev. Lett.* **1996**, *76*, 1501.
(28) Jakubek, Z. J.; Hui, Q.; Takami, M. *Phys. Rev. Lett.* **1997**, *79*, 629.
(29) Bartelt, A.; Close, J. D.; Federmann, F.; Quaas, N.; Toennies, J. P. *Phys. Rev. Lett.* **1996**, *77*, 3525.
(30) Federmann, F.; Hoffmann, K.; Quaas, N.; Close, J. D. *Phys. Rev. Lett.* **1999**, *83*, 2548.
(31) Mella, M.; Colombo, M. C.; Morosi, G. *J. Chem. Phys.* **2002**, *117*, 9695.
(32) Wada, A.; Takayanagi, T.; Shiga, M. *J. Chem. Phys.* **2003**, *119*, 5478.
(33) Lewerenz, M.; Schilling, B.; Toennies, J. P. *Chem. Phys. Lett.* **1993**, *206*, 381.
(34) Knuth, E. L.; Henne, U. *J. Chem. Phys.* **1999**, *110*, 2664.
(35) Vrakking, M. J. J. *Rev. Sci. Instrum.* **2001**, *72*, 4084.
(36) Braun, A.; Drabbels, M. *Rev. Sci. Instrum.* **2005**, *76*, 113103.
(37) Zhu, L. C.; Johnson, P. *J. Chem. Phys.* **1991**, *94*, 5769.
(38) Mullerdethlefs, K.; Sander, M.; Schlag, E. W. *Chem. Phys. Lett.* **1984**, *112*, 291.
(39) Knuth, E.; Schilling, B.; Toennies, J. P. *Proceedings of the 19th International Symposium on Rarefied Gas Dynamics;* Oxford University Press: London, 1995; p 270.
(40) Loginov, E.; Rossi, D.; Drabbels, M. *Phys. Rev. Lett.* **2005**, *95*, 163401.
(41) Pickering, J. C.; Zilio, V. *Eur. Phys. J. D* **2001**, *13*, 181.
(42) Merkt, F. *Annu. Rev. Phys. Chem.* **1997**, *48*, 675.
(43) Loock, H. P.; Beaty, L. M.; Simard, B. *Phys. Rev. A* **1999**, *59*, 873.
(44) Carlsson, J.; Jonsson, P.; Sturesson, L. *Z. Phys. D* **1990**, *16*, 87.
(45) Takahashi, Y.; Sano, K.; Kinoshita, T.; Yabuzaki, T. *Phys. Rev. Lett.* **1993**, *71*, 1035.
(46) Dupontroc, J. *Z. Phys. B: Condens. Matter* **1995**, *98*, 383.
(47) Jakubek, Z. J.; Takami, M. *Chem. Phys. Lett.* **1997**, *265*, 653.
(48) Reho, J.; Higgins, J.; Lehmann, K. K.; Scoles, G. *J. Chem. Phys.* **2000**, *113*, 9694.
(49) Reho, J.; Higgins, J.; Callegari, C.; Lehmann, K. K.; Scoles, G. *J. Chem. Phys.* **2000**, *113*, 9686.
(50) Frisch, M. J.; Trucks, G. W.; Schlegel, H. B.; Scuseria, G. E.; Robb, M. A.; Cheeseman, J. R.; Montgomery, J. A., Jr.; Vreven, T.; Kudin, K. N.; Burant, J. C.; Millam, J. M.; Iyengar, S. S.; Tomasi, J.; Barone, V.; Mennucci, B.; Cossi, M.; Scalmani, G.; Rega, N.; Petersson, G. A.; Nakatsuji, H.; Hada, M.; Ehara, M.; Toyota, K.; Fukuda, R.; Hasegawa, J.; Ishida, M.; Nakajima, T.; Honda, Y.; Kitao, O.; Nakai, H.; Klene, M.; Li, X.; Knox, J. E.; Hratchian, H. P.; Cross, J. B.; Bakken, V.; Adamo, C.; Jaramillo, J.; Gomperts, R.; Stratmann, R. E.; Yazyev, O.; Austin, A. J.; Cammi, R.; Pomelli, C.; Ochterski, J. W.; Ayala, P. Y.; Morokuma, K.; Voth, G. A.; Salvador, P.; Dannenberg, J. J.; Zakrzewski, V. G.; Dapprich, S.; Daniels, A. D.; Strain, M. C.; Farkas, O.; Malick, D. K.; Rabuck, A. D.; Raghavachari, K.; Foresman, J. B.; Ortiz, J. V.; Cui, Q.; Baboul, A. G.; Clifford, S.; Cioslowski, J.; Stefanov, B. B.; Liu, G.; Liashenko, A.; Piskorz, P.; Komaromi, I.; Martin, R. L.; Fox, D. J.; Keith, T.; Al-Laham, M. A.; Peng, C. Y.; Nanayakkara, A.; Challacombe, M.; Gill, P. M. W.; Johnson, B.; Chen, W.; Wong, M. W.; Gonzalez, C.; Pople, J. A. *Gaussian 03*, revision D.01; Gaussian Inc.: Wallingford, CT, 2004.
(51) Boys, S. F.; Bernardi, F. *Mol. Phys.* **1970**, *19*, 553.
(52) Le Roy, R. J. *LEVEL 7.7: A Computer Program for Solving the Radial Schrödinger Equation for Bound and Quasibound Levels*; University of Waterloo Chemical Physics Research Report CP-661, 2005; see the "Computer Programs" link at http://leroy.uwaterloo.ca.
(53) Schwarz, K. W. *Adv. Chem. Phys.* **1975**, *33*, 1.
(54) Miertus, S.; Scrocco, E.; Tomasi, J. *Chem. Phys.* **1981**, *55*, 117.